Peristaltic-Ciliary Flow of A Casson Fluid through An Inclined Tube

Saravana Ramachandran[1], Kuppalapalle Vajravelu [2*], K. V. Prasad[3], S. Sreenadh[4]

[1]Department of Mathematics, Madanapalle Institute of Technology & Science, Madanapalle 517 325, India.
[2]Department of Mathematics, University of Central Florida, Orlando, Florida 32816, USA.
[3]Department of Mathematics, VSK University, Vinayaka Nagar, Ballari-583 105, Karnataka, India
[4]Department of Mathematics, Sri Venkateswara University, Tirupati 517 502, India.

[*]Email: Kuppalapalle.Vajravelu@ucf.edu

Abstract

The paper is concerned with the peristaltic-ciliary transport of a viscoplastic fluid (Casson fluid) through an inclined cylindrical tube. The peristalsis-cilia induced motion is analysed in the moving frame of reference under the lubrication approximations. Solutions to the flow characteristics petering to yielded and unyielded regions are obtained. The effects of various physical parameters on the axial velocity, the pumping characteristics, the pressure rise, and the frictional force over one wavelength, along with the trapping phenomenon are presented through graphs. Further, the peristaltic flow and peristaltic-ciliary flow results are compared. It is noticed that the axial velocity and the size of trapping bolus in the unplug flow region decrease with an increase in the yield stress. In addition, the axial velocity and the axial pressure gradient in the peristaltic-ciliary pumping are higher than those in the peristaltic pumping.

Keywords: peristalsis-cilia flow, trapping phenomena, Casson fluid, inclined tube, pressure gradient.
2010 MSC classification number: 76D05.

1. INTRODUCTION

The peristaltic pumping of biological fluids through smooth muscle tubes of physiological systems such as oesophagus, stomach, intestines, bile duct, ureter, small blood vessels, male reproductive tract have been extensively studied because of its applications to living body systems, transport of contamination free industrial fluids, design of biomedical and biomechanical instruments. A few studies on the peristaltic flow under the consideration of lubrication approach are available in the literature [1],[2],[3],[4],[5],[6].

The researchers are paying attention to study the peristaltic transport of microorganisms like spermatozoa and ovum. At the time of ovulation the ovum is extruded onto the surface of ovary near the ovarian end of the oviduct and is sucked in the oviduct because of the sweeping motion of the finger like projections called cilia generating a metachronal wave together with the activity of peristalsis of the tubal smooth muscles surrounding them. Several investigations have been examined in ciliary transport. For a detailed exposition see [7],[8],[9],[10]. The combined occurrence of peristalsis and metachronal wave generates a peristalsis-ciliary flow [11],[12],[13],[13]. Ashraf et al. [14] investigated the linear viscous fluid motion in the human fallopian tube due to ciliary and peristaltic muscular activity.

The rheology of Casson fluid model with yield stress exhibits the behaviour of blood and is suitable for describing the steady state shear behaviour of some real materials like printing ink, apple sauce, tomato puree, orange juice (for details see Ref. [15]). Srivastava and Srivastava [16] addressed the peristaltic pumping of blood through a circular non-uniform tube, consisting of a Casson fluid in the core and a Newtonian fluid in the peripheral regions. Later, Misra and Pandey [17] reported the transport of this two layered fluid model in a channel. Mernone et al. [18] applied the perturbation method in terms of the amplitude ratio for the peristaltic propulsion of a Casson fluid through a symmetrical channel. Nagarani and Sarojamma [19] investigated the peristaltic pumping of a Casson fluid with two yield stress planes under the asymmetric conditions of the channel. Later, Hayat et al. [20] examined the impact of convective boundary conditions and Soret and Dufour effects on the peristaltic transport of a Casson fluid in an asymmetric channel. Siddiqui et al. [21] presented

*Corresponding author
Received January 3^{rd}, 2021, Revised March 2^{nd}, 2021, Accepted for publication March 12^{th}, 2021. e-ISSN: 2549-2896, DOI:10.5614/cbms.2021.4.1.3

the transport of a Casson fluid in a tube by the action of cilia. They found that the number of circulations of the closed streamlines decrease as the width of plug increase.

The investigation on the behaviour of biofluids in an inclined geometry is very important in the connection of physiological systems and their functioning. Saravana et al. [22] examined the peristaltic motion of Rabinowitsch fluid in an inclined symmetric channel with the consequences of temperature distribution and compliant walls. The authors observed that an increase in the inclination angle decrease the velocity and the temperature fields of the shear thickening fluid, but the velocities of the shear thinning and Newtonian fluids increase.

In view of the above investigations, we examine the peristaltic-ciliary motion of an incompressible visco-plastic fluid (Casson fluid) characterised by the yield stress in an inclined tube. The closed form solutions for both yielded and unyielded regions are obtained. The effects of various physical parameters on both the yielded and unyielded regions are discussed through graphs and the salient physical features of the biological model are brought out.

2. Model formulation and Solution

Consider a peristaltic-ciliary Casson fluid flow through a two-dimensional uniform tube with inlet mean radius 'a' inclined at an angle β with the horizontal. The cylindrical coordinate system for the axisymmetric tube is used to analyse the flow. The *Z*-axis and *R*-axis are taken along and normal to the tube respectively.

We assume that the uniform tube wall has infinite sinusoidal wave train of propagations with a constant speed 'c' and the inner surface is in line with a mucous membrane layer consisting of secretory and ciliated cells. The peristaltic cyclic contractions and the sweeping motions of the cilia tips are in continuity.

Thus, the combined occurrences of peristalsis (sinusoidal wave) and the effects of swaying motions of the cilia tips (without any loss of generality we assume that the envelope of the cilia tips forming the metachronal wave acts as an extensible wall) and propagates by producing the peristalsis-ciliary travelling wave of the form (for details see [14] and [23]).

$$H(X,t) = a + b\sin\Big(\frac{2\pi}{\lambda}(Z-ct)\Big) + Ab\cos\Big(\frac{2\pi}{\lambda}(\kappa(Z-ct))\Big)\sin\Big(\frac{2\pi}{\lambda}(Z-ct)\Big), \tag{1}$$

where b, λ and t indicate the amplitude, wave length and time respectively. A (A <<1) is the amplitude of the metachronal cilia wave, Ab is the maximum variation of the material particles and κ is a constant.
The constitutive equations for the Casson fluid model are

$$\begin{aligned} \sqrt{\tau} - \sqrt{\tau_0} = \sqrt{\dot{\gamma}} \quad \text{for} \quad \tau > \tau_0, \\ \dot{\gamma} = 0 \quad \text{for} \quad \tau \le \tau_0, \end{aligned} \tag{2}$$

where τ indicates the shear stress, τ_0 and μ are respectively, the yield stress and the viscosity of the fluid, $\dot{\gamma}$ is the rate of shear strain.
Let us choose the transformation from the laboratory frame coordinates (*R*, *Z*) to wave frame coordinates (*r*, *z*) through

$$z = Z - ct; \quad r = R; \quad u = U; \quad p(z) = P(Z,t); \quad \psi = \Psi - \frac{r^2}{2}; \quad h(z) = H(Z,t). \tag{3}$$

in which (*U, W*) indicate the radial and axial velocity components in the (*R, Z*) directions and (*u, w*) indicate the radial and axial velocity components in the (*r, z*) directions. *P* and *p* are the pressures in the fixed and the wave frames respectively. Ψ and ψ are the stream functions in the fixed and the wave frames respectively. *h* is the time independent deformable travelling wave. The physical model of the peristaltic-ciliary flow in the wave frame of reference is as shown in Figure 1. The equations governing the axisymmetric cylindrical polar coordinates in wave frame of reference are

$$\frac{1}{r}\frac{\partial}{\partial r}(ru) + \frac{\partial w}{\partial r} = 0, \tag{4}$$

$$\rho\Big(u\frac{\partial w}{\partial r} + w\frac{\partial w}{\partial z}\Big) = -\frac{\partial p}{\partial z} + \frac{1}{r}\frac{\partial}{\partial r}(r\tau_{rz}) - \frac{\partial}{\partial z}(\tau_{zz}) + \rho g sin\beta, \tag{5}$$

$$\rho\Big(u\frac{\partial u}{\partial r} + w\frac{\partial u}{\partial z}\Big) = -\frac{\partial p}{\partial r} - \frac{1}{r}\frac{\partial}{\partial r}(r\tau_{rr}) - \frac{\partial}{\partial z}(\tau_{rz}) - \rho g cos\beta, \tag{6}$$

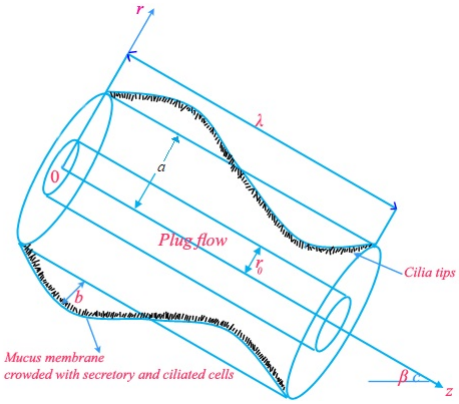

Figure 1: Physical model in the wave frame of reference

In order to non-dimensionalize the equations, we use

$$r' = \frac{r}{a}; \quad r'_0 = \frac{r_0}{a}; \quad z' = \frac{2\pi z}{\lambda}; \quad w' = \frac{w}{c}; \quad u' = \frac{\lambda u}{2\pi ac}; \quad t' = \frac{2\pi ct}{\lambda}; \quad \phi = \frac{b}{a}; \quad \tau'_0 = \frac{\tau_0}{\mu(\frac{a}{c})};$$
$$\tau'_{rz} = \frac{\tau_{rz}}{\mu(\frac{a}{c})}; \quad \psi = \frac{\psi}{a^2c}; \quad P' = \frac{2\pi a^2}{\lambda\mu c}P; \quad Q' = \frac{Q}{\pi a^2 c}; \quad F'_\lambda = \frac{F_\lambda \mu}{\lambda c}; \quad \epsilon = \frac{2\pi a}{\lambda}; \quad h' = \frac{h}{a}; \tag{7}$$
$$Re = \frac{ca}{\gamma}; \quad \gamma = \frac{\mu}{\rho}; \delta = \frac{2\pi a}{\lambda}; \quad F = \frac{\gamma c}{ga^2}.$$

where the stream function ψ is defined as $w = \frac{1}{r}\frac{\partial \psi}{\partial r}; u = -\frac{1}{r}\frac{\partial \psi}{\partial z}$; τ_0 is the yield stress; Q is the volume flow rate, F_λ is the frictional force at the wall across a wave length and F is the body force parameter.
The set of non-dimensional equations pertaining to the flow, under the assumptions of long wave length and small Reynolds number reduce to (dropping the prime symbols)

$$\frac{1}{r}\frac{\partial}{\partial r}(r\tau_{rz}) = -\frac{\partial p}{\partial z} + \frac{sin\beta}{F}, \tag{8}$$

where

$$(\tau_{rz})^{\frac{1}{2}} = \begin{cases} \left(-\frac{\partial w}{\partial r}\right)^{\frac{1}{2}} + \tau_0^{\frac{1}{2}}, & \tau \geq \tau_0, \\ 0, & \tau \leq \tau_0. \end{cases}$$

The non-dimensional boundary conditions are

$$\tau_{rz} \quad \text{is finite at} \quad r = 0, \tag{9}$$
$$\left.\begin{array}{ll} \psi = & 0 \\ \frac{\partial w}{\partial r} = & \frac{1}{r}\frac{\partial \psi}{\partial r} \end{array}\right\} \text{at} \quad r = 0, \tag{10}$$
$$w = -1 \quad \text{at} \quad r = h = 1 + \phi \sin z + \epsilon\phi \sin(\kappa z). \tag{11}$$

Solving the equation (8) together with the boundary conditions (9) – (11), we obtain

$$w = \frac{2\sqrt{2}}{3}\tau_0^{(\frac{1}{2})}\sqrt{P+f}\left(r^{\frac{3}{2}} - h^{\frac{3}{2}}\right) - \left(\frac{P+f}{4}\right)(r^2 - h^2) - \tau_0(r-h) - 1, \quad \text{for} \quad r_0 \leq r \leq r_h \tag{12}$$

in which $P = -(\frac{\partial p}{\partial z})$ and $f = \frac{\sin\beta}{F}$
Applying the condition,

$$\frac{\partial w}{\partial r} = 0, \quad \text{at} \quad r = r_0 \tag{13}$$

we obtain the upper limit of the plug region as $r_0 = \frac{2\tau_0}{P+f}$.
Also, we introduce the condition $\tau_{rz} = \tau_h$ at $r = h$ (as in Vajravelu et al. [23]), which leads to $P = \frac{2\tau_h}{h} - f$.

$$\text{Hence} \quad \frac{r_0}{h} = \frac{\tau_0}{\tau_h} = \tau, \quad \text{for} \quad 0 < \tau < h \tag{14}$$

Using the relation (14) together with $r = r_0$ in Equation (12), we obtain the velocity of the plug, given by

$$w_p = \Big(\frac{P+f}{2}\Big)\Big(-\frac{1}{6}r_0^2 + hr_0 + \frac{1}{2}h^2 - \frac{4}{3}r_0^{\frac{1}{2}}h^{\frac{3}{2}}\Big) - 1, \quad \text{for} \quad 0 \le r \le r_0 \tag{15}$$

The solutions in terms of the stream functions are found by integrating Equations (12) and (15) with the conditions $\psi_p = 0$ at $r = 0$ and $\psi = \psi_p$ at $r = r_0$. They are

$$\psi_p = \Big(\Big(\frac{P+f}{2}\Big)\Big(-\frac{1}{6}r_0^2 + hr_0 + \frac{1}{2}h^2 - \frac{4}{3}r_0^{\frac{1}{2}}h^{\frac{3}{2}}\Big) - 1\Big)\frac{r^2}{2}, \quad \text{for} \quad 0 \le r \le r_0 \tag{16}$$

and

$$\psi = \Big(\Big(\frac{P+f}{2}\Big)\Big(\frac{8}{21}r_0^{\frac{1}{2}}r^{\frac{7}{2}} - \frac{4}{6}r^2r_0^{\frac{1}{2}}h^{\frac{3}{2}} - \frac{r^2}{8}(r^2-2h^2) - \frac{r^2}{6}(2rr_0-3hr_0) + \frac{r_0^4}{168} - \frac{r^2}{2}, \quad \text{for} \quad r_0 \le r \le h \tag{17}$$

Also, the volume flux q through cross-section in the wave frame of reference has the form

$$q = 2\Big(\int_0^{r_0} w_p r dr + \int_{r_0}^{h} w r dr\Big) = \frac{P+f}{8}\Big(1 - \frac{16}{7}\tau^{\frac{1}{2}} + \frac{4}{3}\tau - \frac{1}{21}\tau^4\Big)h^4 - h^2, \tag{18}$$

The non-dimensional instantaneous volume flow rate $Q(X,t)$ in the fixed frame of reference between the wall and the central line is given by $Q = q + h^2$
From Equation 18, we have

$$\frac{\partial p}{\partial z} = \frac{-8(q+h^2)}{\Big(1 - \frac{16}{7}\tau^{\frac{1}{2}} + \frac{4}{3}\tau - \frac{1}{21}\tau^4\Big)h^4} + \frac{\sin\beta}{F}, \tag{19}$$

The non-dimensional time averaged flux $\bar{Q}$ over a period $\Big(T = \frac{\lambda}{c}\Big)$ in the fixed frame is given by

$$\bar{Q} = \frac{2}{T}\int_0^T \int_0^H (w+1) r dr dz = q + \int_0^1 h^2 dz, \tag{20}$$

The pressure rise over a wave length is given by

$$\Delta P = \int_0^1 \frac{dp}{dz} dz, \tag{21}$$

Furthermore, the frictional force at the wall across a wave length has the form

$$F_\lambda = \int_0^1 h^2\Big(-\frac{dp}{dz}\Big)dz. \tag{22}$$

3. Results and Discussion

The analytical approximations to the flow characteristics petering to the yielded and unyielded regions of an incompressible viscoplastic fluid have been determined. The influences of the yield stress parameter τ, the metachronal wave parameter ϵ , the inclination parameter β , the Froude number F along with the other emerging parameters on the axial velocity field, pressure rise frictional force over a wavelength, the axial pressure gradient, the trapping bolus, and the characteristics of a developing embryo within a fallopian tubal fluid in the female human fallopian tube associated with the peristaltic-ciliary flow are explored.

The flow characteristic expressions of the unplug flow and the plug flow regions are presented through Equations (12) and (15). The impacts of the emerging parameters on the axial velocity distribution along with the radial position at the sagittal cross section $(r, 0.5)$ are presented in Figures 2-5. In these figures, the

black lines indicate the axial velocity profiles in the unyielded region. Figure 2 illustrates the variation in the velocity field with the yield stress parameter. We noticed that the velocity decreases with a rise in the yield stress . Worth finding in fallopian tube that the functional blockages such as the mucus plug closest to the uterus may cause the infertility because of prevention of egg passage to the sperm or the fertilized egg to the sperm. The elimination of blockage through microsurgical techniques helps in the success of fertilization.

Figure 3 shows the influence of the angle of inclination of the tube on the axial velocity profiles. We observe that the velocity increases with the enhancement of inclination parameter β. The effects of pressure gradient $\left(-\frac{dp}{dx}\right)$ on the velocity distribution are illustrated in Figure 4. We found that the axial velocity increases with increasing P. Figure 5 displays the effects of the peristaltic-ciliary motion and peristaltic motion on the velocity profiles. The axial velocity of peristaltic-ciliary flow is higher compared with that in the peristaltic flow. Further, we notice that the velocity distribution in the plug flow is constant and flatter; whereas the velocity in the yielded region is parabolic.

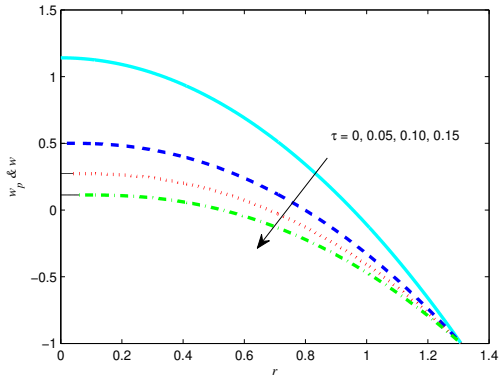

Figure 2: Velocity distribution of τ with $\phi = 0.6$, $\epsilon = 0.1$, $\beta = \frac{\pi}{6}$, $\kappa = 1.5$, $F = 0.5$, $P = 4$

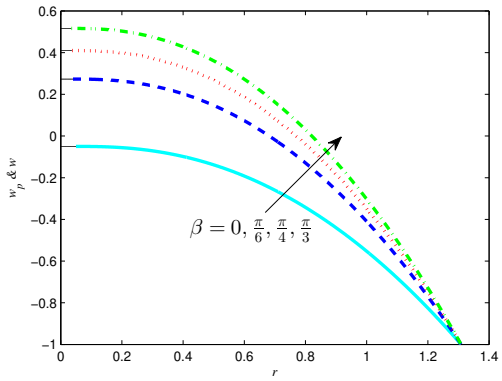

Figure 3: Velocity distribution of β with $\phi = 0.6$, $\epsilon = 0.1$, $\tau = 0.1$, $\kappa = 1.5$, $F = 0.5$, $P = 4$

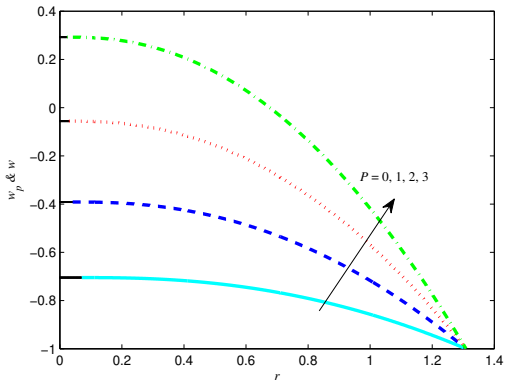

Figure 4: Velocity distribution of P with $\psi = 0.6$, $\beta = \frac{\pi}{4}$ $\epsilon = 0.1$, $\tau = 0.05$, $\kappa = 1.5$, $F = 0.5$

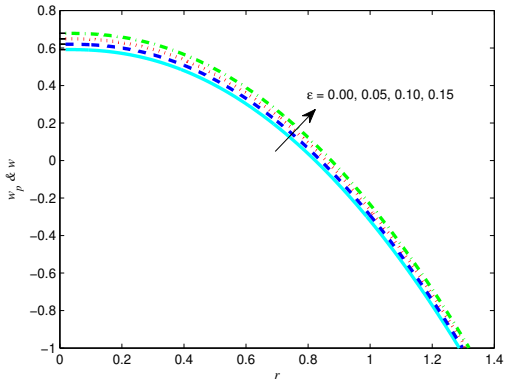

Figure 5: Velocity distribution of ϵ with $\phi = 0.6$, $\beta = \frac{\pi}{4}$, $\tau = 0.05$, $\kappa = 1.5$, $F = 0.5$, $P = 4$

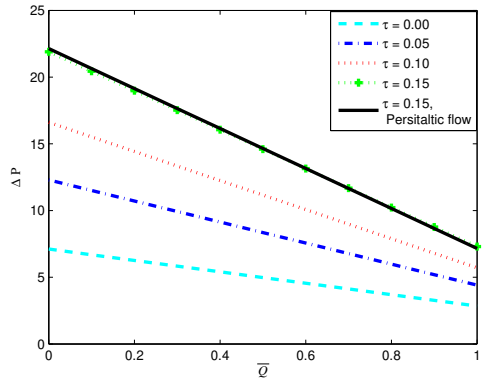

Figure 6: ΔP vs $\bar{Q}$ for different τ at $\phi = 0.4$, $\beta = \frac{\pi}{6}$, $\epsilon = 0.08$, $\kappa = 1.4$, $F = 0.5$

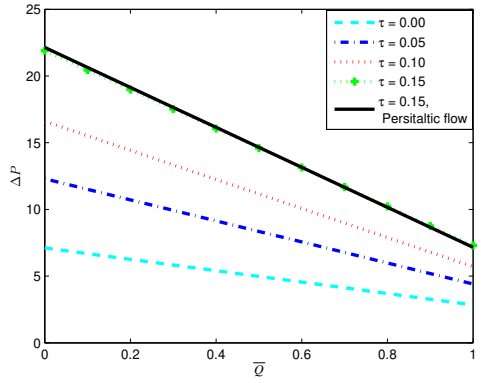

Figure 7: ΔP vs $\bar{Q}$ for different ϵ at $\phi = 0.4$, $\beta = \frac{\pi}{6}$, $\tau = 0.1$, $\kappa = 1.5$, $F = 0.5$

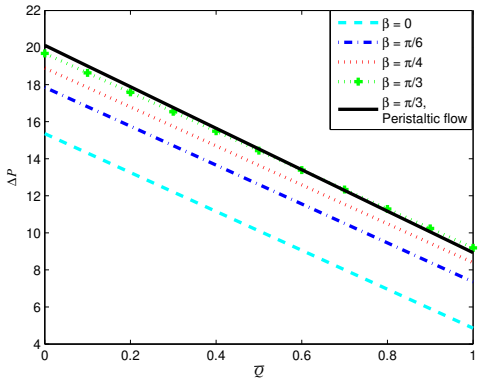

Figure 8: ΔP vs $\bar{Q}$ for different β at $\phi = 0.4$, $\tau = 0.1$,$\epsilon = 0.1$, $\kappa = 1.4$, $F = 0.2$

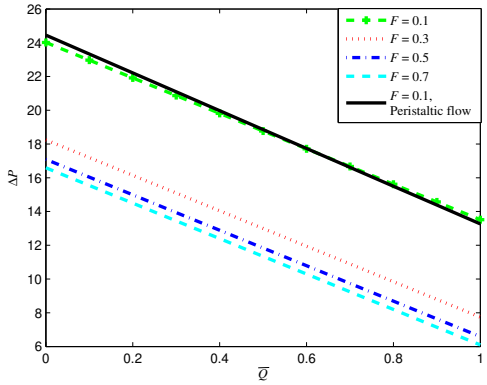

Figure 9: ΔP vs $\bar{Q}$ for different $F = 0.2$ at $\phi = 0.4$, $\beta = \frac{\pi}{3}$, $\tau = 0.1$,$\epsilon = 0.2$, $\kappa = 1.4$

Equation (21) leads to the pressure rise per unit wavelength in terms of time averaged flux $\bar{Q}$. Through Figures 6-9, we study the effects of yield stress parameter τ, metachronal wave parameter ϵ, inclination parameter β and Froude number F on ΔP in terms of $\bar{Q}$. The pressure rise plot provides a comparison of the peristaltic flow $(\epsilon = 0)$ and peristaltic-ciliary flow $(\epsilon \neq 0)$. From Figure 6, we observe that the pumping curves are linear and increases with the yield stress. That is, the pumping efficiency has to be more to push the yield stress fluid $(\tau \neq 0)$ than that of the Newtonian fluid $(\tau = 0)$. It is found that there is a slight variation in pumping curves for $\tau \neq 0$ and $\tau = 0$. Figure 7 exhibits the pumping rate: It decreases with the metachronal wave parameter and the pumping curves coincide at the point $\bar{Q} \approx 0.65$ and an opposite trend is observed for $\bar{Q} > 0.65$. In Figures 8 and 9, we seen that the pumping rate increases with the enhancement in the angle of inclination of the tube and decreases with increasing Froude number. Further, it is evident that the peristaltic flow pumping rate is slightly higher than that in the peristaltic-ciliary flow for $0 \leq \bar{Q} \leq 0.5$ and no variation is found in $0.5 \leq \bar{Q} \leq 0.7$. But the trend is reversed for $\bar{Q} \geq 0.7$. The inclusion of swaying motions of the cilia tips along with the peristaltic propagation causes lessening of pumping rate in the augmented pumping region.

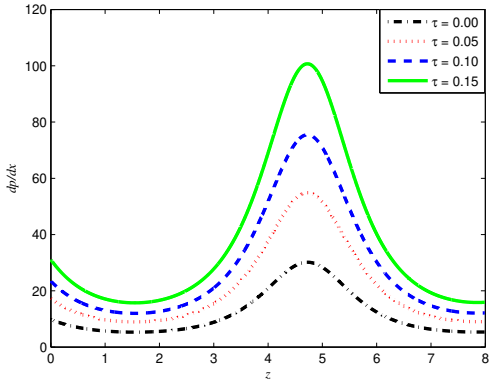

Figure 10: Axial pressure gradient for different τ at $\phi = 0.4$, $\beta = \frac{\pi}{6}$, $\epsilon = 0.02$, $\kappa = 1.2$, $F = 0.5$, $\bar{Q} = -0.1$

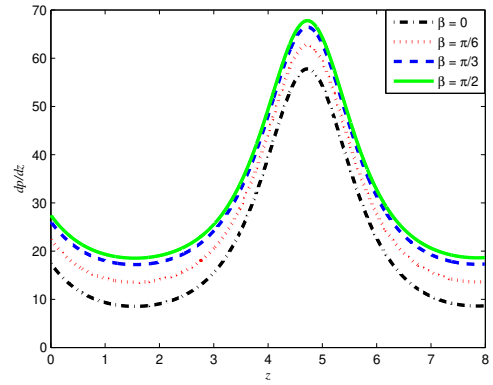

Figure 11: Axial pressure gradient for different β at $\phi = 0.4$, $\tau = 0.06$, $\epsilon = 0.02$, $\kappa = 1.2$, $F = 0.1$, $\bar{Q} = -0.1$

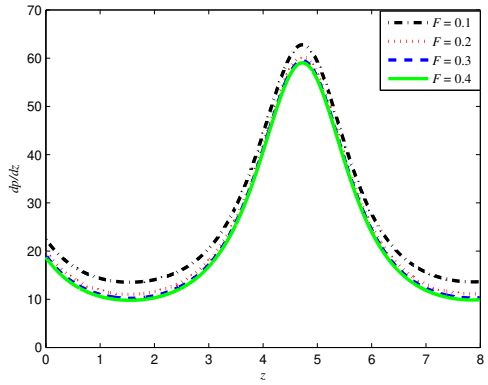

Figure 12: Axial pressure gradient for different F at $\phi = 0.4$, $\tau = 0.06$,$\beta = \frac{\pi}{6}$, $\epsilon = 0.02$, $\kappa = 1.2$, $F = 0.1$, $\bar{Q} = -0.1$

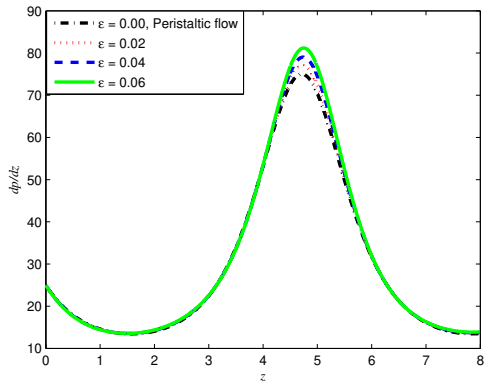

Figure 13: Axial pressure gradient for different ϵ at $\phi = 0.4$, $\tau = 0.1$,$\beta = \frac{\pi}{6}$, $F = 0.2$, $\kappa = 1.2$,$\bar{Q} = -0.1$

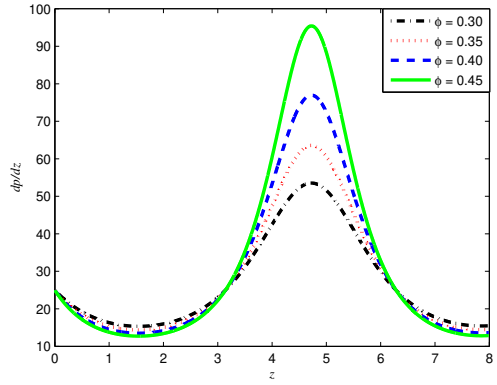

Figure 14: Axial pressure gradient for different ϕ at $\epsilon = 0.02$, $\tau = 0.1$,$\beta = \frac{\pi}{6}$, $F = 0.2$, $\kappa = 1.2$,$\bar{Q} = -0.1$

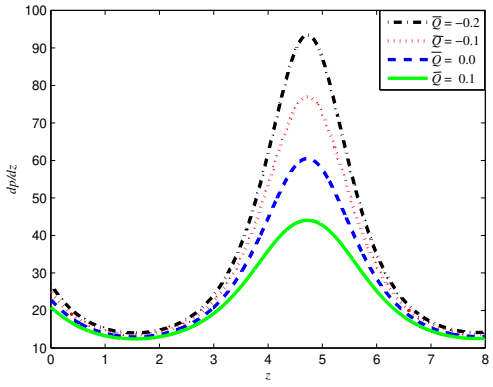

Figure 15: Axial pressure gradient for different $\bar{Q}$ at $\phi = 0.4$, $\epsilon = 0.02$, $\tau = 0.1$,$\beta = \frac{\pi}{6}$, $F = 0.2$, $\kappa = 1.2$

The axial pressure gradient in terms of z is given in Equation (19) and its variations with the various physical parameters are presented in Figures 10 - 15. Figure 10 demonstrates that the magnitude of the pressure gradient is an increasing function of the yield stress, which infer that the pressure gradient is higher for the Casson fluid when compared to that of the Newtonian fluid. From Figures 11 and 12, we see that the amplitude of the axial pressure gradient rises with an increase in the angle of inclination and reduces with the Froude number. Figure 13 illustrates the pressure gradient comparison of the peristaltic and the peristaltic-ciliary flows. The comparison indicates that the peristaltic-ciliary flow has the larger amplitude than that of the peristaltic flow in the fallopian tube. Figure 14 indicates the pressure gradient enhancement with increasing amplitude ratio. In Figure 15, we see that the magnitude of the pressure gradient decreases with an increase in the time averaged flux $\bar{Q}$.

Equation (22) provides the frictional force at the wall F_λ per unit wavelength in terms of $\bar{Q}$. Figures 16-19 are drawn to demonstrate the effects of the yield stress parameter τ, metachronal wave parameter ϵ, inclination parameter β and Froude number F on the F_λ in terms of $\bar{Q}$. The frictional force plot provides the comparison of peristaltic flow $(\epsilon = 0)$ and peristaltic-ciliary flow $(\epsilon \neq 0)$. From Figure 16, we seen that F_λ curves are linear and decrease with increasing yield stress. Further, there is a slight variation in F_λ curves for $(\epsilon \neq 0)$ and $(\epsilon = 0)$. Figure 17 exhibits that the frictional force at the wall decreases with the increase in metachronal wave parameter. In Figures 18 and 19, we seen that the frictional force at the wall decreases with an increase in the angle of inclination of the tube and increases with the Froude number. From these plots, it is clear that the frictional force has quite opposite trend to that of the pressure rise.

The stream function expressions of the plug and unplug flow regions are represented in Equations (16) and (17). The effects of τ, ϵ , β, F, P and the constant κ on the stream line patterns in the unplug flow region are depicted graphically in Figures 20-25. From Figures 20, we infer that the formation of the size of trapping bolus decreases with an increase in the yield stress parameter. In Figures 21, we see that the trapped bolus volume decreases and the trapping zone moves to the left with an increase in ϵ. It indicates that for small Reynolds number, the movements of cilia termed as metachronism shows impact on the stream lines. Figures 22 reveal that the bolus is not formed for $\beta = 0$ (see Figure 22(a)), the development of trapping bolus enhanced, and the trapping zone shifts upwards with the angle of inclination. Figures 23 demonstrate that the trapped bolus volume diminishes with increasing Froude number and the bolus not found for $F = 0.4$ (see Figure 23(d)). Figures 24 depict that the trapping bolus size increases with rising the values of the pressure gradient and the bolus is not formed for $P = 0$ (see Figure 24(a)). Figures 25 show that the trapped bolus decreases with increasing the constant κ.

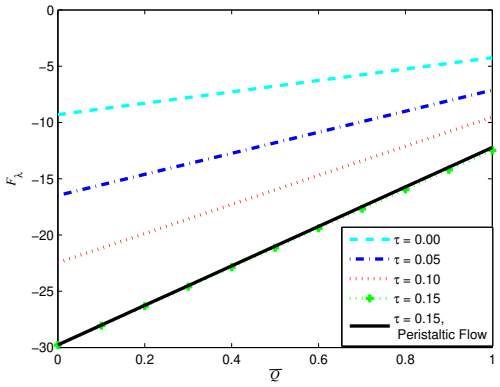

Figure 16: F_λ versus $\bar{Q}$ for different τ at $\phi = 0.6$, $\epsilon = 0.08$, $\beta = \frac{\pi}{6}$, $F = 0.1$, $\kappa = 1.5$

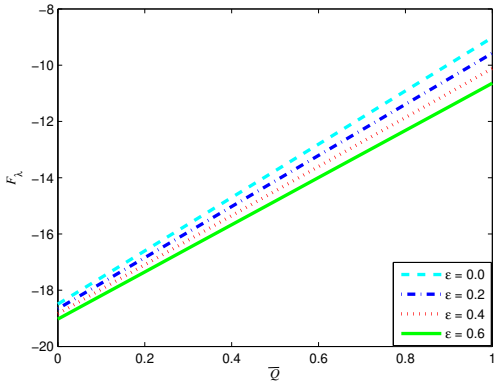

Figure 17: F_λ versus $\bar{Q}$ for different ϵ at $\phi = 0.6$, $\tau = 0.05$, $\beta = \frac{\pi}{6}$, $F = 0.5$, $\kappa = 1.5$

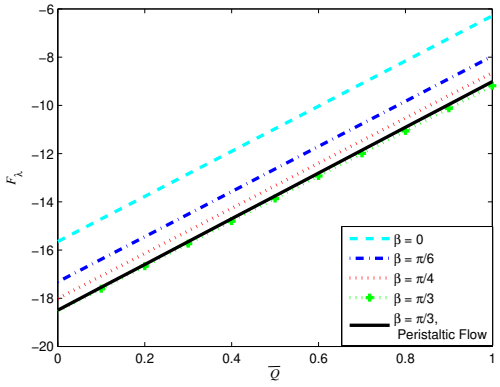

Figure 18: F_λ versus $\bar{Q}$ for different β at $\phi = 0.6$, $\epsilon = 0.08$, $\tau = 0.05$, $F = 0.5$, $\kappa = 1.5$

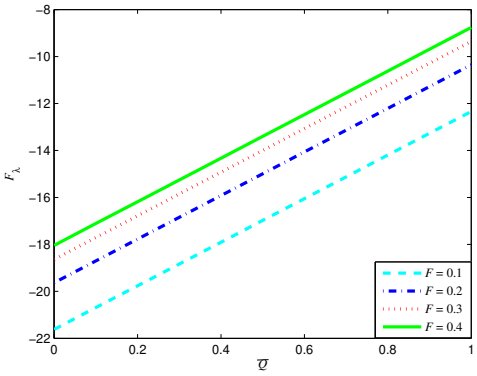

Figure 19: F_λ versus $\bar{Q}$ for different F at $\phi = 0.6$, $\epsilon = 0.1$, $\tau = 0.05$, $\kappa = 1.5$, $\beta = \frac{\pi}{4}$

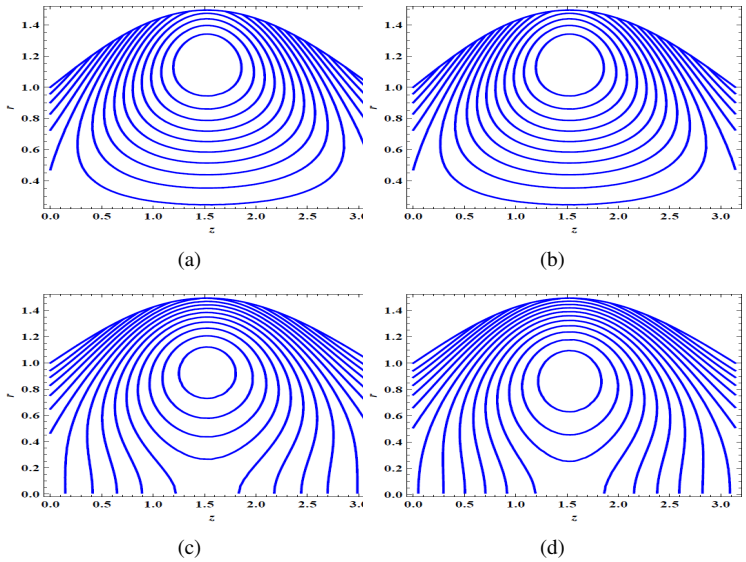

Figure 20: Stream line patterns for (a) $\tau = 0$, (b)$\tau = 0.01$ (c) $\tau = 0.02$ (d)$\tau = 0.03$ with $\phi = 0.5$, $\epsilon = 0.04$, $\kappa = 1.2$, $\beta = \frac{\pi}{6}$, $F = 0.2$, $P = 2$

4. Conclusion

In the present study, we analysed the peristaltic-ciliary flow of a Casson fluid in an inclined tube under the lubrication approximations. The analytical solutions for both the yielded and unyielded regions are obtained. The effects of various physical parameters on both the regions are depicted by plotting graphs. Some interesting findings are presented below.

1. Axial velocity decreases with the yield stress; but increases with a rise in the inclination parameter. The peristalsis-ciliary axial flow characteristics are higher compared to those in the peristaltic flow.
2. Pumping curves are linear and increase with increasing yield stress.
3. Frictional force at the wall decreases due to increase in metachronal wave parameter.
4. Pressure gradient is higher for the Casson fluid compared to that of Newtonian fluid.
5. The size of trapping bolus decreases with increasing yield stress.

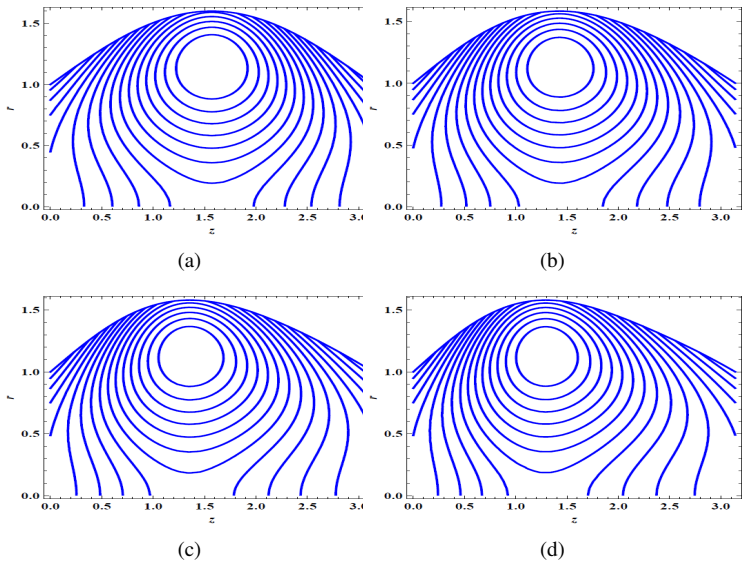

Figure 21: Stream line patterns for (a) $\epsilon = 0.00$, (b) $\epsilon = 0.12$ (c) $\epsilon = 0.18$ (d) $\epsilon = 0.24$ with $\phi = 0.6$, $\beta = \frac{\pi}{6}$, $\tau = 0.02$, $\kappa = 1.2$, $F = 0.2$, $P = 2$

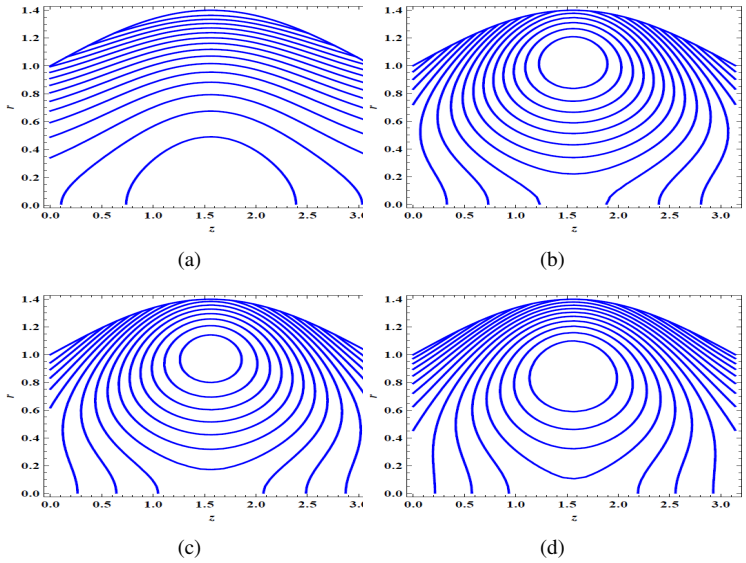

Figure 22: Stream line patterns for (a) $\beta = 0$, (b) $\beta = \frac{\pi}{6}$ (c) $\beta = \frac{\pi}{4}$ (d) $\beta = \frac{\pi}{3}$ with $\phi = 0.4$,$\epsilon = 0.01$, $\tau = 0.01$, $\kappa = 1.2$, $F = 0.2$, $P = 2$

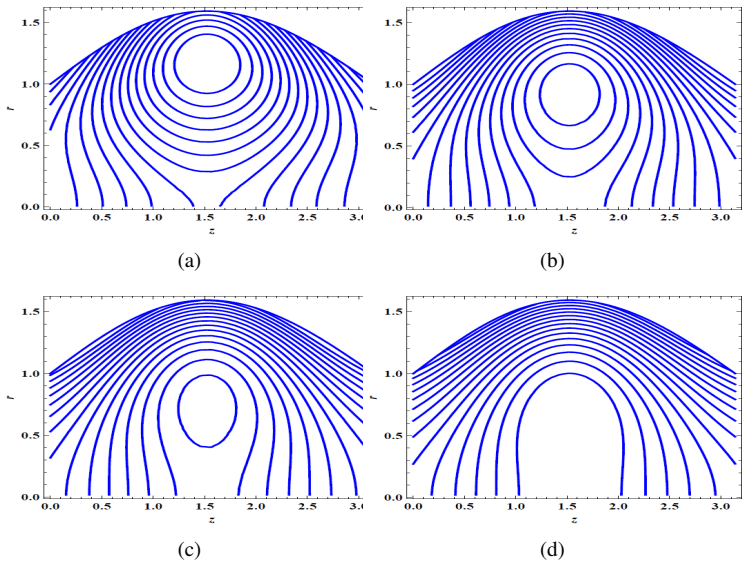

Figure 23: Stream line patterns for (a) $F = 0.1$, (b) $F = 0.2$ (c) $F = 0.3$ (d) $F = 0.4$ with $\phi = 0.4$, $\beta = \frac{\pi}{6}$, $\epsilon = 0.04$, $\tau = 0.03$, $\kappa = 1.2$, $P = 1.5$

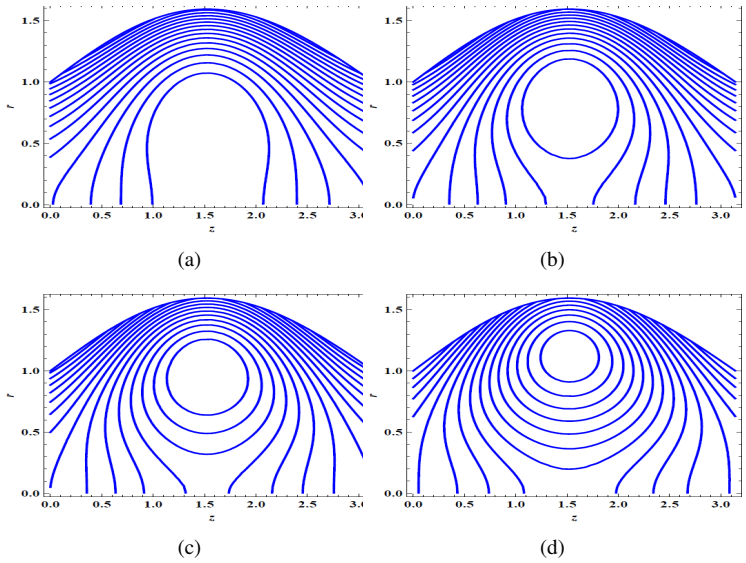

Figure 24: Stream line patterns for (a) $P = 0$, (b) $P = 0.5$ (c) $P = 1$ (d) $P = 2$ with $\phi = 0.4$, $\beta = \frac{\pi}{6}$, $\epsilon = 0.04$, $\tau = 0.03$, $\kappa = 1.2$, $F = 0.2$

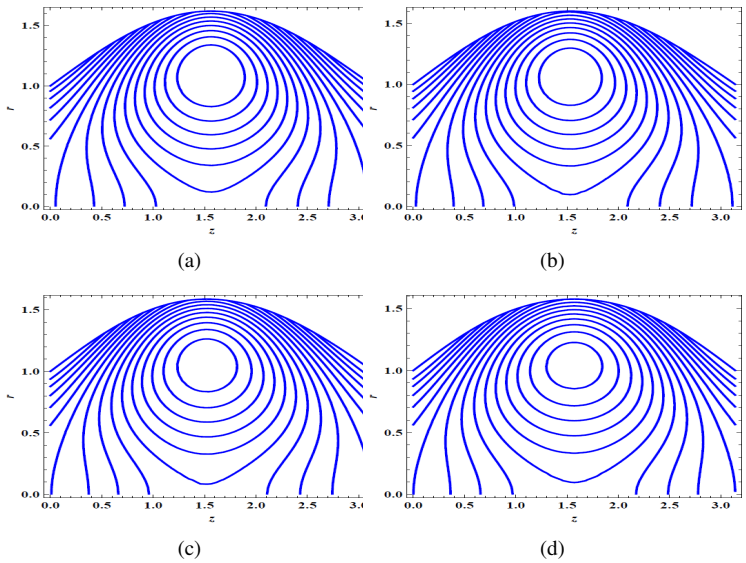

Figure 25: Stream line patterns for (a) $\kappa = 0.4$, (b) $\kappa = 1.0$ (c) $\kappa = 1.4$ (d) $\kappa = 2$ with $\phi = 0.6$, $\beta = \frac{\pi}{6}$, $\epsilon = 0.04$, $\tau = 0.01$, $P = 1.5$, $F = 0.2$

REFERENCES

[1] Shapiro, A.H., Jaffrin, M.Y. and Weinberg, S.L., Peristaltic pumping with long wave lengths at low Reynolds number, Journal of Fluid Mechanics, 37(4), pp. 799-825, July 1969.

[2] Ramachandra Rao, A. and Mishra, M., Peristaltic transport of a power-law fluid in a porous tube, Journal of Non-Newtonian Fluid Mechanics, 121(2-3), pp. 163-174, 2004. https://doi.org/10.1016/j.jnnfm.2004.06.006.

[3] Hayat, T., and Ali, N., A mathematical description of peristaltic hydromagnetic flow in a tube, Applied Mathematics and Computation, 188(2), pp. 1491–1502, 2007. https://doi.org/10.1016/j.amc.2006.11.035.

[4] Saravana, R., Sreenadh, S., Kumar, P.R. and Babu, V.R., Peristaltic pumping of Ellis fluid through a flexible tube with complete slip effects, Journal of Naval Architecture and Marine Engineering, 17(2), pp. 79-88. 2020. https://doi.org/10.3329/jname.v17i2.49559.

[5] Vajravelu, K., Sreenadh, S. and Saravana, R., Combined influence of velocity slip, temperature and concentration jump conditions on MHD peristaltic transport of a Carreau fluid in a non-uniform channel with wall properties, Applied Mathematics and Computation, 225, pp. 656-676, 2013. https://doi.org/10.1016/j.amc.2013.10.014.

[6] Saravana, R., Hemadri Reddy, R., Suresh Goud, J., and Sreenadh, S., MHD peristaltic flow of a Hyperbolic tangent fluid in a non-uniform channel with heat and mass transfer, IOP Conf. Series: Materials Science and Engineering 263, pp. 1-15, 2017. https://doi.org/10.1088/1757-899x/263/6/062006.

[7] Lardner, T.J. and Shack, W.J., Cilia transport, The bulletin of mathematical biophysics, 34(3), pp.325-335. 1972. https://doi.org/10.1007/BF02476445.

[8] Nadeem, S., Munim, A., Shaheen, A. and Hussain, S., Physiological flow of Carreau fluid due to ciliary motion, AIP Advances, 6(3), Article ID: 035125, 2016. https://doi.org/10.1063/1.4945270.

[9] Nadeem, S. and Sadaf, H., Metachronal wave of cilia transport in a curved channel, Zeitschrift für Naturforschung A, 70(1), pp. 33-38, 2015. https://doi.org/10.1515/zna-2014-0117

[10] Maiti, S. and Pandey, S.K., Rheological fluid motion in tube by metachronal waves of cilia. Applied Mathematics and Mechanics, 38(3), pp.393-410, 2017. https://doi.org/10.1007/s10483-017-2179-8.

[11] Leese, H.J., The formation and function of oviduct fluid. Reproduction, 82(2), pp. 843-856, 1988. https://doi.org/10.1530/jrf.0.0820843.

[12] Croxatto, H.B., Physiology of gamete and embryo transport through the fallopian tube. Reproductive biomedicine online, 4(2), pp. 160-169, 2002. https://doi.org/10.1016/S1472-6483(10)61935-9.

[13] Lyons, R.A., Saridogan, E. and Djahanbakhch, O., The reproductive significance of human Fallopian tube cilia. Human reproduction update, 12(4), pp. 363-372. 2006. https://doi.org/10.1093/humupd/dml012.

[14] Ashraf, H., Siddiqui, A.M. and Rana, M.A., Fallopian tube assessment of the peristaltic-ciliary flow of a linearly viscous fluid in a finite narrow tube. Applied Mathematics and Mechanics, 39(3), pp. 437-454. 2018. https://doi.org/10.1007/s10483-018-2305-9.

[15] Bird, R.B., Dai, G.C. and Yarusso, B.J., The rheology and flow of viscoplastic materials. Reviews in Chemical Engineering, 1(1), pp. 1-70, 1983. https://doi.org/10.1515/revce-1983-0102.

[16] Srivastava, L.M. and Srivastava, V.P., Peristaltic transport of blood: Casson model - II. Journal of Biomechanics, 17(11), pp. 821-829, 1984. https://doi.org/10.1016/0021-9290(84)90140-4.

[17] Misra, J.C. and Pandey, S.K., Peristaltic transport of blood in small vessels: study of a mathematical model. Computers & Mathematics with Applications, 43(8-9), pp. 1183-1193, 2002. https://doi.org/10.1016/S0898-1221(02)80022-0.

[18] Mernone, A.V., Mazumdar, J.N. and Lucas, S.K., A mathematical study of peristaltic transport of a Casson fluid. Mathematical and Computer Modelling, 35(7-8), pp. 895-912, 2002. https://doi.org/10.1016/S0895-7177(02)00058-4.

[19] Nagarani, P. and Sarojamma, G., 2004. Peristaltic transport of a Casson fluid in an asymmetric channel. Australasian Physics & Engineering Sciences in Medicine, 27(2), pp. 49-59, 2004. https://doi.org/10.1007/BF03178376.

[20] Hayat, T., Yasmin, H. and Al-Yami, M., Soret and Dufour effects in peristaltic transport of physiological fluids with chemical reaction: A mathematical analysis. Computers & Fluids, 89, pp. 242-253, 2014. https://doi.org/10.1016/j.compfluid.2013.10.038.

[21] Siddiqui, A.M., Farooq, A.A. and Rana, M.A., A mathematical model for the flow of a Casson fluid due to metachronal beating of cilia in a tube. The Scientific World Journal, 2015. Article ID:487819, pp. 1-12, https://doi.org/10.1155/2015/487819.

[22] Saravana, R., Vajravelu, K. and Sreenadh, S., Influence of compliant walls and heat transfer on the peristaltic transport of a Rabinowitsch fluid in an inclined channel. Zeitschrift für Naturforschung A, 73(9), pp.833-843, 2018. https://doi.org/10.1515/zna-2018-0181.

[23] Vajravelu, K., Sreenadh, S. and Ramesh Babu, V., Peristaltic transport of a Herschel–Bulkley fluid in an inclined tube. International Journal of Non-Linear Mechanics, 40(1), pp. 83 – 90, 2005. https://doi.org/10.1016/j.ijnonlinmec.2004.07.001.

[24] Wakeley, P.W., Optimisation and Properties of Gamete Transport, Ph. D. dissertation, University of Birmingham, pp. 139–166, 2008.